Published in "Optics Express 21(13): 15121–15130, 2013"
which should be cited to refer to this work.

A Bell-Bloom experiment with polarization-modulated light of arbitrary duty cycle

I. Fescenko,[1,2,*] **P. Knowles,**[1] **A. Weis,**[1] **and E. Breschi**[1]

[1]*Physics Department, University of Fribourg, Chemin du Musée 3, 1700 Fribourg, Switzerland*
[2]*Laser Center of the University of Latvia, Zellu Str. 8, Riga, Latvia*
**iliafes@gmail.com*

Abstract:
We report on a study of polarization-modulation experiments on the $4 \rightarrow 3$ hyperfine component of the D_1 transition in Cs vapor contained in a paraffin-coated cell. The laser beam's polarization was switched between left- and right-circular polarization at a rate of 200 Hz. Variations of the transmitted light power were recorded while varying the amplitude of a transverse magnetic field. The power shows electromagnetically induced transparency (EIT) resonances when the atomic Larmor frequency matches a harmonic of the modulation frequency. We made a quantitative study of the resonance amplitudes with square-wave modulations of various duty cycles, and find an excellent agreement with recent algebraic model predictions.

References and links

1. W. Bell and A. Bloom, "Optically driven spin precession," Phys. Rev. Lett. **6,** 280–281 (1961).
2. V. Schultze, R. IJsselsteijn, T. Scholtes, S. Woetzel, and H. Meyer, "Characteristics and performance of an intensity-modulated optically pumped magnetometer in comparison to the classical M_x magnetometer," Opt. Express **20,** 14201–14212 (2012).
3. N. W. Gawlik, L. Krzemien, S. Pustelny, D. Sangla, J. Zachorowski, M. Graf, A.O. Sushkov, and D. Budker, "Nonlinear Magneto-Optical Rotation with Amplitude-Modulated Light," Appl. Phys. Lett. **88,** 131108 (2006).
4. V. Acosta, M. P. Ledbetter, S. M. Rochester, D. Budker, D. F. Jackson-Kimball, D. C. Hovde, W. Gawlik, S. Pustelny, and J. Zachorowski, "Nonlinear magneto-optical rotation with frequency-modulated light in the geophysical field range," Phys. Rev. A **73,** 053404 (2006).
5. M. Huang, and J. C. Camparo, "Coherent population trapping under periodic polarization modulation: Appearance of the CPT doublet," Phys. Rev. A **85,** 012509 (2012).
6. A. Ben-Kish, and M.V. Romalis, "Dead-Zone-Free Atomic Magnetometry with Simultaneous Excitation of Orientation and Alignment Resonances," Phys. Rev. Lett. **105,** 193601 (2010).
7. Z. D. Grujić, and A. Weis, "Atomic magnetic resonance induced by a amplitude-, frequency-, or polarization-modulated light," arXiv:1305.6574 [physics.atom-ph] (May 2013).
8. E. B. Aleksandrov, "Optical manifestations of the interference of nondegenerate atomic states," Sov. Phys. Usp. **15,** 436–451 (1973).
9. E. B. Alexandrov, M. Auzinsh, D. Budker, D. F. Kimball, S. M. Rochester, and V. V. Yashchuk, "Dynamic effects in nonlinear magneto-optics of atoms and molecules: review," J. Opt. Soc. Am. B **22,** 7–20 (2005).
10. N. Castagna, and A. Weis, "Measurement of longitudinal and transverse spin relaxation rates using the ground-state Hanle effect," Phys. Rev. A **84,** 053421 (2011).
11. T. Petelski, M. Fattori, G. Lamporesi, J. Stuhler, and G.M. Tino,"Doppler-free spectroscopy using magnetically induced dichroism of atomic vapor: a new scheme for laser frequency locking," Eur. Phys. J. D **22,** 279–283 (2003).

12. G. Wasik, W. Gawlik, J. Zachorowski, and W. Zawadzki, “Laser frequency stabilization by Doppler-free magnetic dichroism,” Appl Phys. B **75,** 613–619 (2002).
13. N. Castagna, G. Bison, G. Di Domenico, A. Hofer, P. Knowles, C. Macchione, H. Saudan, and A. Weis, “A large sample study of spin relaxation and magnetometric sensitivity of paraffin-coated Cs vapor cells,” Appl. Phys. B **96,** 763–772 (2009).
14. E. Breschi, Z. Grujić, and A. Weis, “In-situ calibration of magnetic field coils using free-induction decay of atomic alignment,” submitted to Appl. Phys. B (2013).
15. E. Breschi and A. Weis, “Ground-state Hanle effect based on atomic alignment,” Phys. Rev. A **86,** 053427 (2012).
16. E. B. Alexandrov, M. V. Balabas, A. S. Pasgalev, A. K. Vershovskii, and N. N. Yakobson, “Double-resonance atomic magnetometers: from gas discharge to laser pumping,” Laser Phys. **251,** 244–251 (1996).

1. Introduction

In 1961 Bell and Bloom have shown [1] that amplitude modulated circularly polarized optical resonance radiation can induce magnetic resonance transitions in the atomic ground state. The effect manifests itself as Lorentzian-shaped resonances in the light power transmitted by the atomic vapor, when the amplitude B of an applied static transverse (with respect to the light propagation direction) magnetic field is varied. Resonances occur when the Larmor frequency $\omega_L = \pm g|B|$ matches the intensity modulation frequency ω_{mod}, where g is the gyromagnetic factor of the atomic ground state.

When modeling the effect, Bell and Bloom used a sinusoidal amplitude modulation. Using, on the other hand, a square wave intensity modulation that contains all harmonics of the fundamental frequency ω_{mod} will lead to a richer spectrum in which resonances occur at $\omega_L = \pm m\,\omega_{\text{mod}}$. In recent years, phase-sensitive detection was used to record such amplitude-modulation resonance spectra with an improved signal/noise ratio (compared to Bell and Bloom’s low-pass filtered detection), either by direct lock-in detection of the transmitted power [2] or in combination with polarization analysis [3].

Related magnetic resonance spectra can also be obtained by modulating either the light frequency [4] or polarization [5,6]. Weis and Grujić [7] have recently developed analytical expression for the positions, amplitudes, and shapes of magnetic resonances produced by amplitude-, frequency-, or polarization-modulation with arbitrary duty cycle. Such modulation schemes have been referred to generically as phase resonances [8,9].

The underlying physics of phase resonances is the creation of atomic spin polarization by optical pumping, where the light modulation is equivalent to a modulation of the optical pumping efficiency. The magnetic field induces a precession of the induced polarization and the resonant structure of the transmitted intensity results from the interplay of the periodic polarization creation process and the field-induced polarization dynamics. In the simplest implementation, the same light beam is used to create the spin polarization and to detect its alteration by the magnetic interaction. The magnetic resonance lines can be observed on one hand in the DC (i.e., low-pass filtered) power transmitted by the medium, and on the other hand as oscillations of the transmitted power at harmonics of the modulation frequency. In the latter case, the resonances can be recorded by a phase-sensitive analysis of the power. This detection scheme will not be addressed here.

The present paper reports on a study of the simplest variant of polarization-modulation resonances that uses a single laser beam and low-pass filtered detection of the transmitted laser power. This scheme is equivalent to the original Bell-Bloom experiment, in which the sinusoidal power modulation has been replace by a square wave polarization modulation.

There is a growing interest in magnetic sublevel spectroscopy using amplitude-, frequency-, or polarization-modulation, which is motivated by the development of so-called ‘magnetically-silent’ magnetometers. In contrast to the classical double resonance magnetometers [16], in which an oscillating magnetic field drives transitions between magnetic sublevels, magneti-

cally silent magnetometers are all-optical devices, which do not require the application of an oscillating field. In general, all-optical devices have distinctive advantages for compact sensor geometries, or for operating sensors under harsh experimental conditions, such as in vacuum or near a high voltage conductor. The signals reported here may find application for a novel type of silent magnetometer.

2. Model

In a recent paper, algebraic expressions for the line shapes of magnetic resonance spectra induced by circular polarization-modulated light in a transverse magnetic field $\vec{B}$ have been derived [7]. The basic experimental configuration of polarization modulation spectroscopy is shown on the left of Fig.1. The beam of a single mode laser whose frequency is actively stabilized to an atomic transition traverses an atomic medium of length L. A polarization modulator is used to periodically flip the helicity $\xi(t)$ of the circular light polarization at frequency ω_{mod}. It was shown in [7] that the magnetic field dependence of the transmitted light power, $P(\omega_L \propto |\vec{B}|)$, contains both time-independent and time-dependent contributions.

The time-independent Bell-Bloom type signals of interest here consist of a magnetic field independent background and an infinite series of absorptive resonances given by

$$P(\omega_L) = (1-\kappa_0 L)\,P_0 + \alpha\kappa_0 L\,\frac{P_0^2}{P_S}\sum_{m=-\infty}^{\infty} g_m^2\,\mathscr{L}_m(\omega_L) \tag{1}$$

$$\equiv (1-\kappa_0 L)\,P_0 + \sum_{m=-\infty}^{\infty} A_m\,\mathscr{L}_m(\omega_L)\,, \tag{2}$$

where P_0 and P are the laser power before and after the cell, respectively, κ_0, the resonant absorption coefficient of the vapor, and α, the atomic polarization (orientation) analyzing power introduced in [10], which depends on the atomic transition to which the laser frequency is tuned. The factors $A_m \propto g_m^2$ represent the amplitudes of the Lorentzian resonances

$$\mathscr{L}_m(\omega_L) = \frac{\gamma^2}{(m\omega_{\mathrm{mod}} - \omega_L)^2 + \gamma^2}\,, \tag{3}$$

centered at $\omega_L = m\,\omega_{\mathrm{mod}}$, where the linewidth γ represents the (transverse) coherence relaxation rate, assumed in [7] to be equal to the longitudinal relaxation rate. The constants g_m are the Fourier coefficients of the polarization modulation function $\xi(t)$. We note that Eq. (2) was derived for optically thin media ($\kappa_0 L \ll 1$) in the low power limit, for which the resonance amplitudes are proportional to P_0^2. In Eq. (1), P_S denotes the saturation power for optical pumping, which is related to the optical pumping rate γ_p by $\gamma_p = \gamma P_0/P_S$.

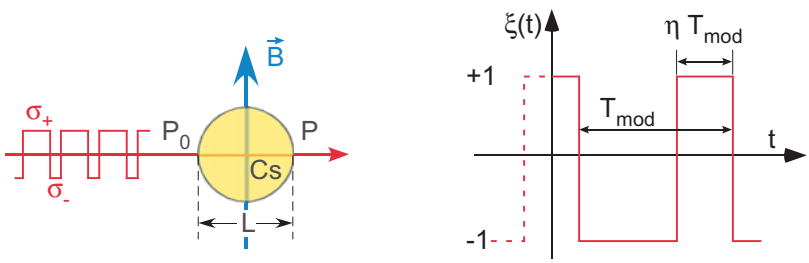

Fig. 1. Left: schematic principle of polarization-modulation experiment. Right: the time-symmetric polarization modulation function $\xi(t)$ with representation of duty cycle η.

2.1. *The polarization modulation function*

In the experiments, the helicity ξ of the light is periodically switched between σ_+ and σ_-, corresponding to $\xi = +1$ and $\xi = -1$. The right part of Fig. 1 shows the corresponding modulation function with period $T_{\mathrm{mod}} = 2\pi\,\omega_{\mathrm{mod}}^{-1}$ for an arbitrary duty cycle η, corresponding to the fractional time during which the light is σ_+-polarized. The model calculations [7] were performed for a symmetric, $\xi(t) = \xi(-t)$, modulation function so that the Fourier series is composed purely of cosines

$$\xi(t) = \sum_{m=-\infty}^{+\infty} g_m(\eta)\,\cos(m\omega_{\mathrm{mod}}\,t)\,, \tag{4}$$

with η-dependent coefficients

$$g_{m=0}(\eta) = 2\eta - 1 \quad \text{and} \quad g_{m\neq 0}(\eta) = \frac{2}{\pi}\,\frac{\sin(\pi\,m\,\eta)}{m}\,. \tag{5}$$

With arbitrary duty cycles, the resonance amplitudes become η-dependent, and we define relative resonance amplitudes as

$$R_m(\eta) = \frac{A_m(\eta)}{A_1(0.5)} = \frac{g_m^2(\eta)}{g_1^2(0.5)} = \begin{cases} \left[\dfrac{\pi(2\eta-1)}{2}\right]^2 & m = 0 \quad (6) \\[2ex] \dfrac{\sin^2(\pi m\eta)}{m^2} & m \neq 0 \quad (7) \end{cases}$$

For a 50% duty cycle (η = 0.5) the only non-zero amplitudes are $R_m(0.5) = m^{-2}$ with odd m. In this symmetric modulation case, one thus expects to observe no zero field (m = 0) Hanle resonance.

3. Experimental apparatus

Figure 2 shows a schematic diagram of the experimental apparatus. The experiments were performed with light from an 894 nm diode laser (Toptica DL100L, distributed feedback laser) whose frequency was actively locked to the $F_g = 4 \rightarrow F_e = 3$ hyperfine transition of the cesium D_1 line using a Doppler-free dichroic atomic vapor laser lock (DAVLL) technique [11, 12].

The laser beam was carried by a polarization maintaining fiber to the experiment proper and split by a polarizing beam splitter cube into two beams of approximately equal intensity. The power of one beam, monitored by a photodiode $\mathrm{PD_{ref}}$, served as a reference sensor for background subtraction and common mode noise suppression. The polarization of the second beam was modulated between right (σ_-) and left (σ_+) handed circular polarization by an electro-optic modulator (Thorlabs, model EO-AM-NR-C1 with model HVA200 driver). The EOM was driven by a square wave with adjustable duty cycle delivered by a waveform generator (Keithley, model 3390). The degree of circular polarization of the two orthogonal polarization states ($\sigma_\pm$) was better than 95%. The transverse intensity profile of the laser beam was determined by the EOM's 2 mm clear aperture.

The polarization-modulated beam traversed an evacuated 30 mm diameter spherical glass cell containing cesium vapor at ambient temperature. The inner walls of the cell were coated with a thin layer of paraffin to reduce spin depolarization by wall collisions. The properties and preparation procedure of the cells are described in [13]. The cell was mounted in an ≈1 m long double-layer cylindrical μ-metal shield without end-caps and with an innermost diameter of ≈200 mm. Two pairs of rectangular coils in Helmholtz configuration and a solenoid mounted inside the shield served to apply a magnetic field in an arbitrary direction and to compensate residual magnetic fields. Coil calibration and residual field compensation procedures

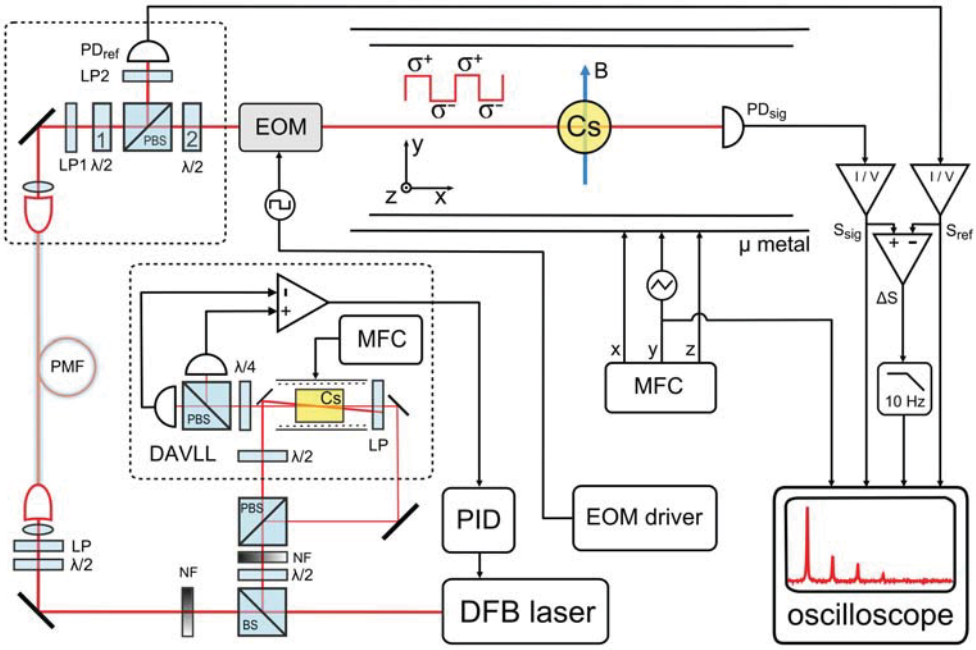

Fig. 2. Block diagram of experimental apparatus. BS: beam splitter; DFB laser: distributed feedback laser; EOM: electro-optic modulator; I/V: transimpedance amplifier; LP: linear polarizer; NF: neutral density filter; MFC: magnetic field control PBS: polarizing beam splitter; PD_{sig} and PD_{ref}: signal and reference photodiodes; PID: proportional-integral-differential feedback controller; PMF: polarization maintaining fiber.

are described in [14]. The current through the Helmholtz coil used to vary the field B_y in the horizontal plane (cf. Fig. 2) was controlled by a ramp from a waveform generator (Agilent, model 33220A) via a voltage-controlled current source. The scan speed $d\nu_L/dt$ was on the order of 20–40 Hz/s in order to avoid signal distortions due to the long relaxation time (tens of ms) of the spin polarization in the coated cells [10].

The light transmitted through the cell was detected by the signal photodiode PD_{sig}. The components in the top left box of Fig. 2 served to control the power in the experiment and in the reference channel as follows: the polarizer LP1 defines the polarization after the fiber, the half-wave plate 1 controls the power P_0 sent the experiment and the half-wave plate 2 optimizes the production of circularly polarized light by the EOM. Finally, the polarizer LP2 is used to balance S_{sig} and S_{ref} when the laser frequency is tuned away from the absorption line. The signals from the photodiodes PD_{ref} and PD_{sig} were amplified by transimpendance amplifiers (Femto, model DLPCA-200) with an effective feedback resistor of 1 MΩ.

The electronic difference signal $\Delta S = S_{sig} - S_{ref}$ is low-pass filtered by an SRS (model SIM965) analog filter with a cutoff frequency of 10 Hz to suppress the time dependent signal components. This differential detection scheme improves the S/N ratio by more than an order of magnitude and allows observation of up to $m = 21$ harmonics.

4. Experimental results

All experiments were carried out at a fixed σ_+/σ_- modulation frequency $\omega_{mod}/2\pi = 200$ Hz, chosen such as to minimize both the overlap of adjacent resonance lines and the total field

domain to be examined.

4.1. *Spectra*

Polarization modulation spectra were recorded by scanning the magnetic field B_y over a range covering the resonances at $\omega_L = (0\ldots5)\omega_{\mathrm{mod}}$. The signals $\mathrm{S_{sig}}$, $\mathrm{S_{ref}}$, $\Delta\mathrm{S}$ and the magnetic field controlling voltage ramp were recorded by a digital oscilloscope (Agilent, model DSO6014A) and averaged over 20 minutes, yielding the time averaged signals $\overline{\Delta\mathrm{S}} = \langle \mathrm{S_{sig}} - \mathrm{S_{ref}} \rangle$. According to Eq. (2), the experimental signal $\overline{\Delta\mathrm{S}}$ is related to the theoretical expression by the proportionality

$$\overline{\Delta\mathrm{S}}(\eta) \propto P(\omega_L) - P_0 = -\kappa_0 L P_0 + \sum_{m=-\infty}^{\infty} A_m(\eta)\,\mathscr{L}_m(\omega_L)\,, \tag{8}$$

and thus consists of a series of equi-spaced resonances centered at $\omega_L = m\omega_{\mathrm{mod}}$ superposed on a field independent background.

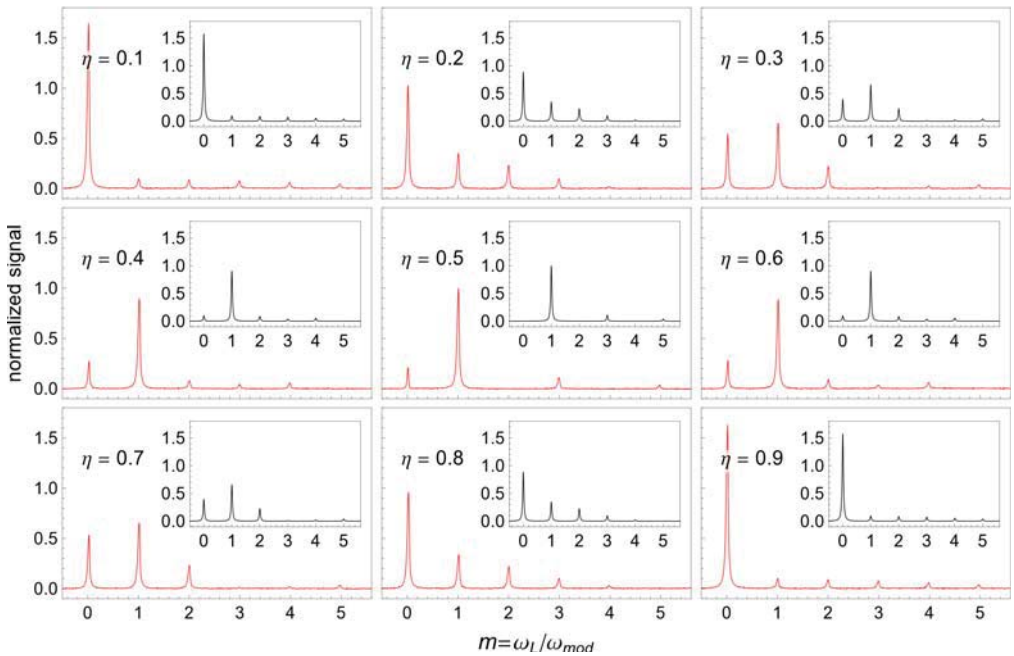

Fig. 3. Polarization modulation spectra represented as magnetic field dependence of the transmitted laser power (incident laser P_0 = 1.0 μW) for different modulation duty cycles η. The insets show the theoretical spectra. Both experimental and theoretical spectra are normalized, after background subtraction, as discussed in the text.

Figure 3 shows a series of experimental spectra for nine different values of the duty cycle η at an incident laser power P_0 = 1.0 μW. Each experimental spectrum was fitted by a sum of absorptive Lorentzian functions on a constant background, according to Eq. (8). The fitted background is subtracted in the spectra displayed in Fig. 3. For the fits we have imposed identical widths on all resonances at positions $\omega_L \neq 0$, while the $\omega_L = 0$ Hanle resonance was allowed a different width. We have found that the Hanle linewidth is smaller than the other resonances, a fact that we will address in more detail in Sec. 4.4. The fits thus yield the amplitudes $A_m^{\mathrm{exp}}(\eta)$ of all resonances, as well as two linewidths.

The spectra shown in the figure are normalized to the fitted amplitude $A_1^{\mathrm{exp}}(0.5)$ of the $m = 1$ resonance at $\omega_L = \omega_{\mathrm{mod}}$ observed with 50% duty cycle. The magnetic field, i.e., Larmor frequency dependence is represented in units of the modulation frequency $(m = \omega_L/\omega_{mod})$.

The inset in each plot represents the corresponding theoretical spectrum, plotted with relative amplitudes given by Eqs. (6,7) and linewidths determined from the fits. The identical vertical scales of all spectra allow one not only to appreciate the relative intensities of the harmonic signals for a given value of η, but also the relative intensities of spectra recorded for different values of η. We note the symmetry of the η and $1-\eta$ spectra predicted by the model.

4.2. *Relative amplitudes*

The array of plots shown in Fig. 4 represents the dependence of the relative amplitudes $R_m^{\mathrm{exp}}(\eta) = A_m^{\mathrm{exp}}(\eta)/A_1^{\mathrm{exp}}(0.5)$ of the Hanle resonance (m=0) and the harmonics $m = 1\ldots5$ on the duty cycle η. Data are shown for P_0 = 1 μW and 3 μW, respectively. The experimental amplitudes A_m^{exp} are taken from the fits as described in the previous paragraph. A cosine function is then fitted to the η-dependence of $A_1^{\mathrm{exp}}(\eta)$, and the fit value at η = 0.5 is used to normalize all data.

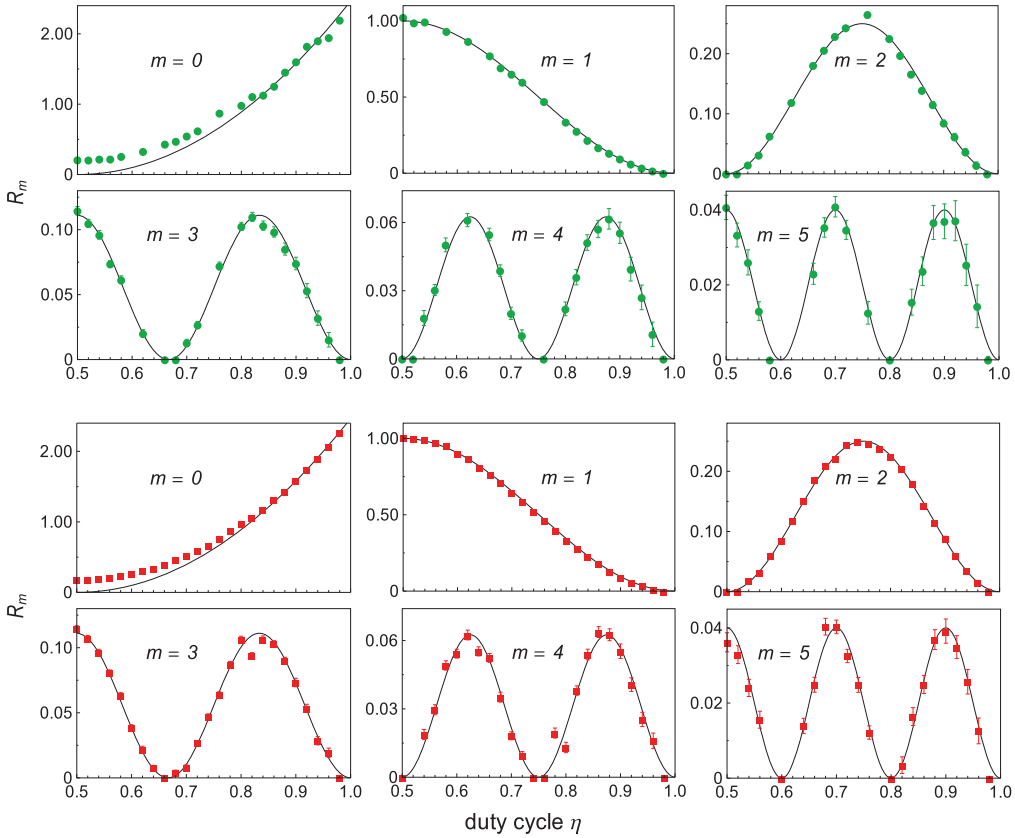

Fig. 4. Dependence of the relative resonance amplitudes on the duty cycle η for the resonances at $m = \omega_L/\omega_{\mathrm{mod}} = 0\ldots5$. Data were recorded with an incident laser power P_0 = 1 μW (top 6 graphs, green dots) and 3 μW (bottom 6 graphs, red squares), respectively. The dots/squares represent the normalized experimental amplitudes and the solid lines show the model predictions.

The solid lines lines represent the η-dependencies given by Eq. (6,7). One sees that, except for the $m = 0$ Hanle resonance, there is an excellent agreement with the model predictions. The slight disagreement of the Hanle data will be addressed in paragraph 4.4 below.

4.3. Power dependence

The model predictions developed in [7] were derived in the low light power limit. Equation (2) shows that in that limit the resonance amplitudes are proportional to P_0^2. In order to ensure that the experiments were carried out within the model's domain of validity, we have studied the dependence of the amplitude $A_1^{\mathrm{exp}}(0.5)$ on the incident laser power P_0. The results are shown in the left part of Fig. 5, together with a polynomial fit. The dashed line in the low power region (shown as inset) represents the $A_1^{\mathrm{exp}}(0.5) \propto P_0^2$ part of the fitted polynomial.

One sees that up to 1 μW, the amplitude has dominantly a quadratic power dependence, while at 3 μW the experimental amplitude is $\approx$2 times smaller than the value from the quadratic extrapolation (dashed line). The model predictions should thus reproduce well the experimental findings up to P_0 = 1 μW, while one might expect some deviations at higher power. However, the experimental results of Fig. 4 show that the relative amplitudes are also well reproduced by the model at 3 μW.

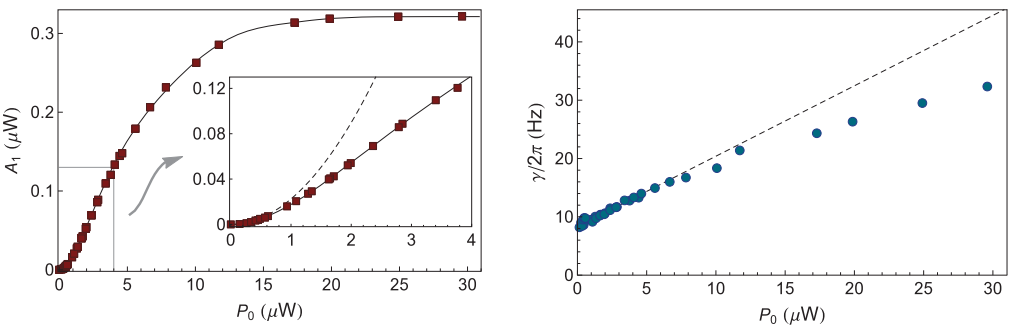

Fig. 5. Left: dependence of the $(m = 1, \eta = 0.5)$-resonance amplitude on the incident laser power P_0. The solid squares are experimental amplitudes and the solid line is a polynomial fit. The inset is a zoom into the low power region. The dashed line represents the quadratic term of the fit. Right: Dependence of the half-width of the $(m = 1, \eta = 0.5)$ resonance on laser power. The dashed line is a linear fit to the data below 6 μW.

We have also performed an experiment with P_0 = 15 μW, i.e., a power level for which the absolute resonance amplitudes show already a strong saturation according to Fig. 5. Analysis of those data (not shown here) reveals still an excellent agreement of the experimental relative amplitudes with the model predictions. We thus conclude that our model predictions give an excellent description of the relative amplitudes up to a (saturating) power of 15 μW, while the absolute amplitudes show a quadratic power dependence only up to 1 μW.

The right part of Fig. 5 shows the power broadening of the $m = 1$ resonance which, as expected, deviates from a linear dependence but in a manner less pronounced than the amplitude saturation behavior shown on the left. One expects that the power broadening is independent of η, since changes in duty cycle do not alter the average power of the atom–light interaction, in contrast to corresponding experiments using amplitude or frequency modulation. This is confirmed by the solid dot data of Fig. 6 below.

4.4. *Hanle resonance*

According to the model predictions of Eq. (5), one expects no $m = 0$ Hanle resonance for a 50% duty cycle modulation. However, the experimental spectrum (graph for $\eta = 0.5$ in Fig. 3) shows a pronounced resonance at $\omega_L = 0$. We believe that this resonance is due to atomic alignment (tensor spin polarization) produced by optical pumping with the circularly polarized beam. Since the model calculations [7] assumed atomic orientation (vector polarization) only, it is clear that they are not able to predict any alignment-based resonance.

Alignment based Hanle resonances excited with linearly polarized light have been studied in detail [15]. The B_y field used in our experiments is orthogonal to the alignment (oriented along the light propagation $\hat{k}$), and the model of [15] predicts the following lineshape for the zero field alignment resonance

$$\mathscr{B}(\omega_L) \propto \frac{\gamma^2}{(2\omega_L)^2 + \gamma^2}\,, \tag{9}$$

i.e., a Lorenzian whose width is half the width of the orientation-based resonances described by Eq. (3), provided that the alignment and orientation relax at the same rate γ. One thus expects that the $m = 0$ Hanle resonance consists of a narrower resonance due to alignment only for $\eta = 0.5$, while for $\eta \neq 0.5$ the Hanle resonance would be formed by a weighted average of two Lorentzians of different widths. We have not attempted to fit two superposed resonances of different widths to the Hanle peaks, but used a single resonance for all values of η.

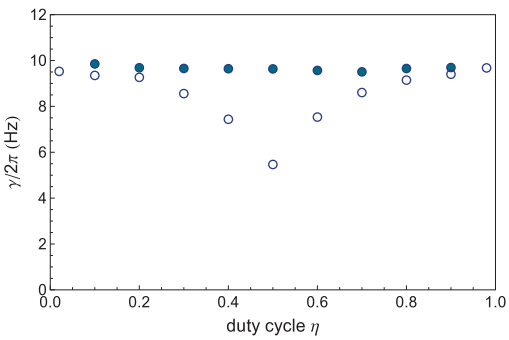

Fig. 6. Dependence of the linewidth $\gamma/2\pi$ of the $m = 0$ Hanle resonances (open dots) and the $m \neq 0$ resonances (solid dots) on the duty cycle η. Data taken at $P_0 = 1.0\ \mu$W.

Based on the above, one expects the width of the Hanle resonance to change with η. The results shown in Fig. 6 confirm this hypothesis. The figure compares the dependence of the $m = 0$ and $m \neq 0$ linewidths on the duty cycle η. While the $m \neq 0$ widths do not depend on η, the Hanle linewidth smoothly evolves from a smaller value at $\eta = 0.5$, to the value of the $m \neq 0$ resonances as η approaches 0 and 1. As discussed in [7], the production and detection of alignment by circularly polarized is less efficient than the production and detection of orientation on the $4 \rightarrow 3$ hyperfine transition. For $\eta \rightarrow 0$ and $\eta \rightarrow 1$ one thus expects the orientation contribution to dominate over the alignment contribution.

5. Summary and conclusion

We have studied polarization modulation resonances on the $4 \rightarrow 3$ hyperfine component of the Cs D_1 transition in a transverse magnetic field. When the light polarization is periodically switched between left- and right-circular polarization we observe a spectrum of resonances at which the vapor's transmission is enhanced. This observation can be interpreted in terms of

electromagnetically induced transparency (EIT), which occurs when the modulation frequency ω_{mod} and the atomic Larmor frequency ω_L fulfill the resonance condition $\omega_L = m\,\omega_{\mathrm{mod}}$. With a 50% modulation duty cycle resonances occur only at odd harmonics m, while for other duty cycles we observe both even and odd harmonics. The amplitudes of the different harmonics have a characteristic oscillatory dependence on the duty cycle that is well described by an algebraic model. At low incident light power, the amplitudes of all harmonics scale with the square of the power and fully saturate (under our conditions) for power levels above 15 μW. We find that our model gives nonetheless a satisfactory description of the *relative* harmonic amplitudes even for saturating power levels. A slight discrepancy between experimental and theoretical signal amplitudes for the $m = 0$ level crossing resonance is traced back to a (small) signal contribution from atomic alignment that is not included in our theory. We are in the process of extending our model calculation to spin-aligned media. This should allow us for a quantitative interpretation of the particular feature of the Hanle resonance.

Acknowledgments

I. Fescenko acknowledges support by Grant 11.133 of the Scientific Exchange Programme (Sciex-NMS^{ch}). E. Breschi acknowledges funding by Ambizione grant PZ00P2_131926 of the Swiss National Science Foundation.